

Momentum-conserving self-gravity in the PHANTOM smoothed particle hydrodynamics code

Parallel dual tree traversal for the symmetric fast multipole method

Yann Bernard¹, Timothée David-Cléris¹, Daniel J. Price^{2,1}, and Mike Y. M. Lau^{3,4}

¹ Univ. Grenoble Alpes, CNRS, IPAG, 38000 Grenoble, France

² School of Physics and Astronomy, Monash University, VIC 3800, Australia

³ Heidelberger Institut für Theoretische Studien, Schloss-Wolfsbrunnenweg 35, 69118 Heidelberg, Germany

⁴ Zentrum für Astronomie der Universität Heidelberg, Astronomisches Rechen-Institut, Mönchhofstr. 12-14, 69120 Heidelberg

Received September 30, 20XX

ABSTRACT

Context. Tree codes that approximate groups of distant particles with multipole expansions are the standard way to accelerate the computation of self-gravity on particles. While momentum-conserving fast multipole methods exist, parallelisation is non-trivial and previous implementations have been limited to self-gravity with fixed softening lengths.

Aims. We aim for a practical, parallel version of Dehnen’s momentum-conserving Cartesian fast multipole method for the computation of the gravitational force in smoothed particle hydrodynamics (SPH) with adaptive gravitational force softening.

Methods. We parallelise the dual tree walk by replicating the node-node interaction on the parents of each leaf node in the tree. While this duplicates work, it greatly simplifies the parallelisation and can be implemented with relatively minor changes from the previous non-conservative force algorithm in PHANTOM. We also adapt the tree opening criterion for adaptive softening lengths, such that all interactions within the softening kernel are handled pairwise (as in SPH) rather than with multipole expansions, also allowing the gravity calculation to be performed alongside the SPH force evaluation.

Results. We demonstrate that the new code conserves linear momentum to machine precision while giving similar force accuracy and computational performance to the previous (non-symmetric) fast multipole method in PHANTOM. The new method also gives better conservation of the angular momentum and orbital phase in a binary polytrope evolution.

Conclusions. The symmetric fast multipole method is now the default for computing self-gravity in the public code.

Key words. gravitation — hydrodynamics — methods: numerical

1. Introduction

In the first applications of Smoothed Particle Hydrodynamics (SPH), Lucy (1977) and Gingold & Monaghan (1977) computed the self-gravity between binary stars modelled as gaseous polytropic spheres by direct $\mathcal{O}(N^2)$ summation. Monaghan & Lattanzio (1985) first accelerated this by interpolating to a grid and using a multigrid algorithm.

Hernquist & Katz (1989) and Benz et al. (1990) unified SPH with hierarchical tree codes, the former authors basing their method on the Barnes & Hut (1986) Oct-tree, where the complexity is reduced to $\mathcal{O}(N \log N)$ by grouping distant particle-particle interactions into fewer ‘particle-node’ interactions based on a critical opening angle between the particle and the size of the distant node. Benz et al. (1990) used a similar algorithm, but based on a nearest-neighbour binary tree rather than an Oct-tree.

These, and similar tree algorithms, with minor variation (e.g. Salmon & Warren 1994), have remained the basis of collisionless N -body and self-gravitating SPH codes ever since (e.g. Steinmetz & Mueller 1993; Dubinski 1996; Springel et al. 2001; Wadsley et al. 2004; Springel 2005; Wetzstein et al. 2009; Hubber et al. 2011; Gafton & Rosswog 2011; Iwasawa et al. 2017; Wadsley et al. 2017; Price et al. 2018; Schaller et al. 2024).

Greengard & Rokhlin (1987) first showed that $\mathcal{O}(N)$ scaling is possible using a Fast Multipole Method (FMM) where particle-node interactions are replaced by symmetric node-node interactions based on a spherical harmonic expansion. However, their algorithm was not widely adopted in astrophysics because it was found to be slower in practice (in particular Capuzzo-Dolcetta & Miocchi 1998 found it to be almost 3 times slower than their tree code; see Dehnen 2014).

A disadvantage of standard tree codes is that forces between particles are not equal and opposite, meaning that linear momentum is only approximately conserved. Dehnen (2000, 2002) modified the fast multipole method to use symmetric Cartesian multipole expansions, which explicitly conserves linear momentum to machine precision (we denote this scheme as SFMM). But remaining practical difficulties are that i) it requires a recursive dual tree walk algorithm to compute the gravitational force, which is inherently serial; and ii) multipole expansion of the Green’s function to date has only been implemented together with Plummer softening using fixed gravitational softening lengths (Springel et al. 2021). The latter is particularly problematic for SPH codes which utilise adaptive gravitational force softening to ensure that the resolution scales in the gas and gravitational force calculations are identical (see e.g. Bate & Burkert 1997; Price & Monaghan 2007).

In this paper, we describe a parallel implementation of Dehnen's momentum-conserving tree code (Dehnen 2000) for the calculation of the gravitational force in the PHANTOM SPH code. Our algorithm is designed to be used with adaptive gravitational force softening and can be performed during the SPH force loop. It is comparable in speed and accuracy with the existing fast multipole method in PHANTOM, and hence now available as the default method for computing self-gravity in PHANTOM.

The paper is organised as follows: Section 2 covers mathematical details about multipole methods for gravitational interactions. Section 3 presents our new parallel symmetric fast multipole method implementation. Section 4 shows the results of this new method compared to the original in both accuracy and performance. Simple and real-conditions setups have both been used to be able to compare the two methods accurately. We discuss in Section 5 with a comparison with conclusions found in the literature. We conclude in Section 6.

2. Multipole methods for gravitational interactions

For a collection of N collisional point mass particles, the gravitational acceleration on a given particle i is given by

$$\mathbf{a}_i = -\mathcal{G} \sum_{j \neq i}^N \frac{m_j}{|\mathbf{x}_i - \mathbf{x}_j|^3} (\mathbf{x}_i - \mathbf{x}_j), \quad (1)$$

where \mathbf{x}_i and \mathbf{x}_j are the position vectors of the target and source particle, and m_j is the mass of the source particle.

For collisionless fluids or self-gravitating gas, the problem is similar except that the medium is a continuous density field where the gravitational potential must be computed from Poisson's equation

$$\nabla^2 \Phi = 4\pi \mathcal{G} \rho(\mathbf{x}). \quad (2)$$

If the continuous density field $\rho(\mathbf{x})$ is represented by a set of particles of fixed mass, Poisson's equation has the solution

$$\Phi_i = -\mathcal{G} \sum_{j=1}^N m_j \phi(|\mathbf{x}_i - \mathbf{x}_j|, \epsilon), \quad (3)$$

where ϕ is the softening kernel, defined such that $\phi \rightarrow 1/r$ outside the compact support radius (typically several r/ϵ). See Price & Monaghan (2007) and Price et al. (2018) for details.

Both Equations (1) and (3), illustrated in the top row of Figure 1, exhibit two key features: i) the force between two particles is equal and opposite, such that the total momentum $\sum_i m_i \mathbf{v}_i$ is conserved; and ii) that computing the acceleration of all N_p particles via Equation (1) requires $O(N^2)$ pairwise force evaluations. In collisionless N-body and hydrodynamics simulations, where $N_p \gtrsim 10^6$, the force evaluation is then counted in trillions of operations using Equation (1). This part of the calculation can quickly fill the whole CPU time budget in a simulation when N_p is rising. Multipole methods aim to reduce the performance disadvantage of this second characteristic while trying to preserve momentum conservation. We will see in the following that the latter needs special treatment to be satisfied.

2.1. Multipole expansion of the gravitational acceleration

In a self-gravitating medium, the solution of Poisson's equation at the position \mathbf{x}_i can be expressed using the Green's function,

G , associated with it as

$$\Phi(\mathbf{x}_i) = - \int \frac{\mathcal{G} \rho(\mathbf{x}_j)}{|\mathbf{x}_i - \mathbf{x}_j|} d^3 \mathbf{x}_j, \quad (4)$$

$$= -\mathcal{G} \int \rho(\mathbf{x}_j) G(\mathbf{x}_j - \mathbf{x}_i) d^3 \mathbf{x}_j, \quad (5)$$

where $G(\mathbf{r}) = 1/|\mathbf{r}|$, making the integral convergent only when convolved with the density field.

Introducing a third position \mathbf{s}_b (to later represent the centre of a node), we can decompose $\mathbf{x}_j - \mathbf{x}_i$ into two new vectors

$$\mathbf{r} \equiv \mathbf{s}_b - \mathbf{x}_i, \quad (6)$$

$$\mathbf{b}_j \equiv \mathbf{x}_j - \mathbf{s}_b, \quad (7)$$

such that \mathbf{r} represents the distance between the particle receiving the force and the node centre and \mathbf{b} represents the distance between a remote particle and the node centre. Assuming that $|\mathbf{r}| \gg |\mathbf{b}_j|$, the Green's function can be approximated by its multipole expansion around \mathbf{b}_j , giving

$$G(\mathbf{x}_j - \mathbf{x}_i) = G(\mathbf{r} + \mathbf{b}_j), \quad (8)$$

$$\simeq \sum_{n=0}^p \frac{1}{n!} \nabla_r^{(n)} G(\mathbf{r}) \cdot \mathbf{b}_j^{(n)}, \quad (9)$$

where $\nabla_r^{(n)}$ denotes the n th gradient with respect to \mathbf{r} and $\mathbf{b}^{(n)}$ is the n -fold tensor product \mathbf{b} . Here we truncated the expansion to order p in powers of $|\mathbf{b}_j|/|\mathbf{r}|$. Using this expansion in the solution of the Poisson equation (Equation 5), the integral can be moved inside the sum, giving

$$\Phi(\mathbf{x}_i) = -\mathcal{G} \int_V \rho(\mathbf{x}_j) G(\mathbf{x}_j - \mathbf{x}_i) d^3 \mathbf{x}_j, \quad (10)$$

$$\simeq -\mathcal{G} \int_V \rho(\mathbf{x}_j) \sum_{n=0}^p \frac{1}{n!} \nabla_r^{(n)} G(\mathbf{r}) \cdot \mathbf{b}_j^{(n)} d^3 \mathbf{x}_j, \quad (11)$$

$$= -\mathcal{G} \sum_{n=0}^p \frac{1}{n!} \underbrace{\nabla_r^{(n)} G(\mathbf{r})}_{D_n} \cdot \underbrace{\left(\int_V \rho(\mathbf{x}_j) \mathbf{b}_j^{(n)} d^3 \mathbf{x}_j \right)}_{Q_n^B}, \quad (12)$$

where D_n denotes the n th derivative of the Green's function and Q_n^B are the moments of the mass distribution. Hence, the gravitational acceleration can then be written as

$$\mathbf{a}_g(\mathbf{x}_i) = -(\nabla_i \phi)(\mathbf{x}_i) \quad (13)$$

$$= \nabla_i \int \mathcal{G} \rho(\mathbf{x}_j) G(\mathbf{x}_j - \mathbf{x}_i) d^3 \mathbf{x}_j, \quad (14)$$

$$= -\mathcal{G} \int \rho(\mathbf{x}_j) \nabla_j G(\mathbf{x}_j - \mathbf{x}_i) d^3 \mathbf{x}_j, \quad (15)$$

$$= -\mathcal{G} \sum_{n=0}^p \frac{1}{n!} D_{n+1} \cdot Q_n^B. \quad (16)$$

In a system of massive particles, as mentioned earlier, the n -th order mass moment created by a set of point-masses in a cartesian volume reduces to

$$Q_n^B = \sum_j m_j \mathbf{b}_j^{(n)}. \quad (17)$$

This expansion means that one can compute a single force vector on the particle i using the multipole of a box that could

contain multiple particles, as depicted in the second row of Figure 1. Depending on the size of the box, this saves a large number of pairwise particle interactions.

When combined with a hierarchical tree built on the particles, we refer to this as the *Multipole Method* (MM). It is the most commonly used method in astrophysics as it typically several orders of magnitude faster than a direct sum. However, in hydrodynamical simulations with millions of particles, computing the multipole expansion on each individual particle, as in the standard Barnes & Hut (1986) algorithm, starts to be prohibitive.

2.2. Fast multipole methods

Fast Multipole Methods (FMM) reduce the number of evaluations of the Green's function to consider only node-node interactions instead of particle-node interactions (third row of Figure 1).

Consider two nodes at each side (i and j) of the force evaluation. The distance vector between the particles i and j , $\mathbf{x}_j - \mathbf{x}_i$ can be decomposed into three by introducing two new points \mathbf{s}_a and \mathbf{s}_b , referring to the centres of the receiving and sending nodes. Keeping \mathbf{b}_j as previously, we additionally define

$$\mathbf{a}_i \equiv \mathbf{x}_i - \mathbf{s}_a, \quad (18)$$

$$\mathbf{r} \equiv \mathbf{s}_b - \mathbf{s}_a, \quad (19)$$

such that

$$\mathbf{x}_j - \mathbf{x}_i = \mathbf{r} + (\mathbf{b}_j - \mathbf{a}_i). \quad (20)$$

This reduces to the previous Multipole Method when taking $a=0$. Under the assumption $|(\mathbf{b}_j - \mathbf{a}_i)| \ll |\mathbf{r}|$ (noting however that the expansion is exact when $\mathbf{a} = \mathbf{b}$), we can perform an expansion with respect to $(\mathbf{b}_j - \mathbf{a}_i)$ instead of only \mathbf{b}_j as done for the standard multipole expansion. Firstly, for two vectors \mathbf{c}, \mathbf{d} multiplying a symmetric tensor T of order larger than n , we have the following identity

$$T \cdot (\mathbf{d} + \mathbf{c})^{(n)} = T \cdot \sum_{k=0}^n \binom{n}{k} \mathbf{d}^{(n-k)} \mathbf{c}^{(k)}. \quad (21)$$

Using this, the Green's function can be expanded according to

$$G(\mathbf{x}_j - \mathbf{x}_i) = G(\mathbf{r} + \mathbf{b}_j - \mathbf{a}_i), \quad (22)$$

$$\simeq \sum_{n=0}^p \frac{1}{n!} \nabla_r^{(n)} G(\mathbf{r}) \cdot (\mathbf{b}_j - \mathbf{a}_i)^{(n)}, \quad (23)$$

$$= \sum_{k=0}^p \frac{(-1)^k}{k!} \mathbf{a}_i^{(k)} \cdot \sum_{n=0}^{p-k} \frac{1}{n!} D_{n+k} \cdot \mathbf{b}_j^{(n)}. \quad (24)$$

Applying the same procedure as previously, we can insert this Green's function into Equation (5), obtaining

$$\phi(\mathbf{x}_i) = \int_V \rho(\mathbf{x}_j) G(\mathbf{x}_j - \mathbf{x}_i) d^3 \mathbf{x}_j, \quad (25)$$

$$\simeq \int_V \rho(\mathbf{x}_j) \sum_{k=0}^p \frac{(-1)^k}{k!} \mathbf{a}_i^{(k)} \cdot \sum_{n=0}^{p-k} \frac{1}{n!} D_{n+k} \cdot \mathbf{b}_j^{(n)} d^3 \mathbf{x}_j, \quad (26)$$

$$= \sum_{k=0}^p \frac{\mathbf{a}_i^{(k)}}{k!} \cdot \underbrace{(-1)^k \sum_{n=0}^{p-k} \frac{1}{n!} D_{n+k} \cdot Q_n^B}_{M_k} \quad (27)$$

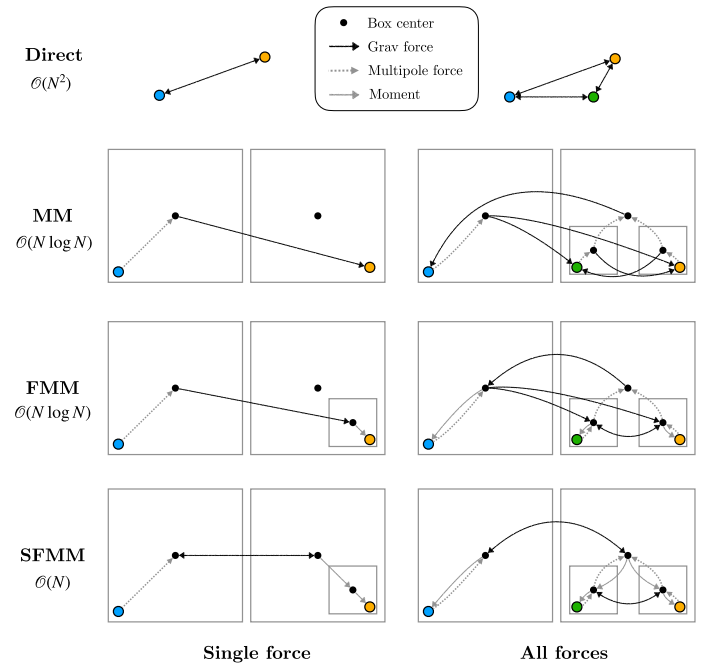


Fig. 1: Multipole methods for computing self-gravity on particles. Left columns shows computation of a single force applied to a target particle, shown in blue. Right column shows forces applied to all particles. The first row shows the direct sum method where every pairwise interaction is computed. The multipole method (second row) uses multipole expansions directly applied on particles of the system to reduce the number of interaction. The fast multipole method (FMM; third row) applies multipole expansion on nodes that hold particles instead to further reduce the number of interactions. The last row corresponds to the symmetric fast multipole method (SFMM) where only pairwise node-node interactions satisfy Newton's third law.

where M_k is a rank- k tensor. The corresponding acceleration is

$$\mathbf{a}_g(\mathbf{x}_i) = \sum_{k=0}^p \frac{\mathbf{a}_i^{(k)}}{k!} \cdot \underbrace{(-1)^k \sum_{n=0}^{p-k} \frac{1}{n!} D_{n+k+1} \cdot Q_n^B}_{dM_k}. \quad (28)$$

where dM_k is the derivative of M_k with respect to r .

Equation (28) implies that the Green's function is required to be evaluated only once per pair of nodes. Depending on the node associations used in the FMM algorithm, different flavours of the same method can be built. For example, the previous self-gravity implementation in PHANTOM used an FMM algorithm that used leaf node-node interactions to reduce the number of long-range interactions by the mean number of particles in a leaf node. This gave a theoretical performance gain of around ten. It also had the advantage of being algorithmically similar to a standard tree code, therefore easy to implement. However, MM and this first FMM flavour do not guarantee that forces between pairs of particles are equal and opposite, as their paths are not identical during the expansion. This results in non-conservation of linear momentum and hence centre-of-mass drift in simulations.

We define the Symmetric Fast Multipole Method (SFMM; fourth row of Figure 1) as the flavour that specifically associates target and source nodes interacting with each other to assure only pairwise long-range forces. This change guarantees that Newton's third law is satisfied by the scheme and therefore that linear momentum is conserved. In principle, node-node interactions

can be shared amongst lower level nodes, reducing the overall algorithmic complexity to $O(N)$, but at the expense of being essentially a serial algorithm.

3. Numerical implementation of a symmetric fast multipole method

Despite the conservation advantage of the SFMM over its siblings, implementing this method in a modern parallel hydrodynamical code is non-trivial. Multipole methods are always associated with hierarchical data structures like trees (kd-tree, binary tree, or oct-tree). In SPH, these structures are additionally used to search for neighbours within the computational domain. A tree walk can check, level by level in a top-down fashion, whether a node in the tree could be a potential neighbour by satisfying a locality criterion. Multipole methods use a similar tree walk with slightly different acceptance criteria.

In PHANTOM, the multipole acceptance criterion (MAC) is expressed as (Dehnen 2000, 2014)

$$\theta = \frac{l_{\text{tgt}} + l_{\text{src}}}{d} < \theta_{\text{crit}}, \quad (29)$$

where l_{tgt} and l_{src} are respectively the size of the target and source node, d is the distance between the two nodes and θ_{crit} is the critical opening angle. The MAC allows nodes to interact if they are well-separated, meaning that their opening angle is below a critical value. This criterion, along with the expansion order, controls the accuracy of the computation. This MAC is already well-suited to find the SFMM symmetric interactions between target and source nodes. However, in addition to this MAC, we check a secondary acceptance criterion given by

$$d < [l_{\text{tgt}} + l_{\text{src}} + R_{\text{kern}} \max(h_{\text{max,tgt}}, h_{\text{max,src}})], \quad (30)$$

where $h_{\text{max,tgt}}$ and $h_{\text{max,src}}$ are respectively the maximum smoothing length inside the target and source node, and R_{kern} is the dimensionless cutoff radius of the smoothing kernel. This latter criterion ensures that every neighbour inside the smoothing kernel of the targeted particles will be handled individually to compute SPH forces and, more importantly here, direct softened gravitational forces (Price et al. 2018). It allows a trivial implementation of adaptive gravitational softening with SFMM without modifying the Green's function presented in Section 2.

Tree nodes should also hold the mass moments generated by the particles inside them. In the current code implementation, these mass moments are computed using Equation (17) for each node during the tree building step from the root to the leaf nodes. This downward calculation appears suboptimal as each node will cycle over its constituent particles multiple times from parent to children. However, the current tree construction uses the centre of mass (first mass moment) as the pivot position to build the kd-tree. Thus, computing the other mass moments in this step is actually the most efficient method. Nevertheless, it can be numerically more efficient to build a geometric tree in certain conditions or specific distributions of particles. In such cases, Equation (A.3) can drastically optimise the mass moment computation by only cycling over particles in leaf nodes and translating moments in a bottom-up fashion.

The key algorithm behind the symmetrisation of the FMM is the dual tree traversal presented in Dehnen (2000). However, it is intrinsically serial. Its recursive nature makes it hard to find an embarrassingly parallel version. Dehnen (2014) used a task-based dual tree traversal algorithm to share the load of the

top-down search between multiple threads in the CPU. The performance results of such a method are dependent on the task scheduling to balance the load between threads. Pathological distribution of particles in the system can lead to an unbalanced tree. Moreover, task-based algorithms are not optimised for modern accelerators like GPUs.

Instead, we chose to duplicate the work per leaf of the tree on each thread to make the algorithm embarrassingly parallel. The work duplication implies that we lose the expected $O(N)$ scaling, giving a $O(N \log N)$ complexity, the same as in standard tree codes, but we gain back momentum conservation with a trivially parallel tree traversal.

Algorithms 1 and 2 describe our new implementation of a dual tree traversal in pseudo-code. The parallel loop in this algorithm is performed on the leaf nodes of the tree according to the following steps:

1. The list of parent nodes of a leaf is retrieved up to the root. To start the dual tree walk, the farthest parent of the leaf (which is always the root) and the root are pushed onto a stack of interactions.
2. The main walk is done by popping the last interaction off the stack and testing its opening angle against the acceptance criterion. If the MAC passes, the two nodes are well separated, the node-node interaction is processed, and the gravitational moments are stored in the parent buffer. If not well-separated, tested nodes are opened, and a flag is set to store subsequent interactions on the stack. At this stage, multiple outcomes are possible depending on the nature of the nodes:
 - (a) If the two nodes are both leaf nodes, the tree cannot be walked anymore. Therefore, all interactions between these two nodes should be computed particle by particle. Hence, the source node particles are stored into a cache that will be used later to compute these short-range interactions.
 - (b) If the two nodes are internal, the next parent node and the two children of the source node are pushed onto the stack. Pushing only the next parent on the sink side guarantees to compute only the interactions needed for the targeted leaf without losing the symmetry. Opening both nodes at the same time also helps to minimise the error by limiting the size difference between nodes (Springel et al. 2021).
 - (c) The intermediate case where one node is a large leaf (shallow in the tree) can be problematic. Following Dehnen (2000) and Springel et al. (2021), these interactions must be handled particle by particle. However, due to the symmetry between sink and source nodes, this can involve a large number of direct sum calculations, ruining the performance benefit of the SFMM. We avoided this by allowing shallow leaf nodes to be tested with deeper nodes in the tree. This lowering method can be applied to both the sink and source sides of the interaction without breaking the symmetry.
3. This process is repeated until the stack is empty. Heuristically, the maximum possible stack size corresponds to the depth of the tree. This way, the memory footprint of this process is small.
4. Lastly, we loop over the list of parent nodes to the leaf, from top to bottom. During this loop, the gravitational moments are summed and translated from parents to children using Equation (A.8) until reaching the leaf node. After this step, the gravitational moments are translated onto individual particle positions to get the long-range force. The cached neigh-

bour list can then be used to compute short-range interactions and SPH forces.

Algorithm 1: Parallel Dual Tree traversal

Data: $\{n_i\}_{i \in [0, n]}$ The tree leaf nodes.
Result: $\{dM_{n_i}\}_{i \in [0, n]}$ accumulated gravitational moments.

```

// Main loop on the leaf nodes
1 for  $n_i$  in parallel do
2   parents = get_leaf_branch( $n_i$ );
3   push (parents(1), root) onto stack;
4   while stacksize > 0 do
5      $p_i, n_s$  = pop stack;
6     check_interactions( $p_i, n_s, dM_{p_i}$ , stack);
7     for  $p_i$  in parents do
8       propagate_to_next_parent( $dM_{n_i}, dM_{p_i}, p_i, p_{i+1}$ );

```

Algorithm 2: check_interactions

Data:
 $\{p_i\}$ target node.
 $\{n_s\}$ source node.
 $\{dM_{p_i}\}$ gravitational moments.
 $\{\text{stack}\}$ stack of interactions to test.

```

1 stackit = false;
2 if  $p_i == n_s$  then
3   stackit = true;
4 else
5   if MAC( $p_i, n_s$ ) then
6     compute_M2L( $dM_{p_i}, p_i, n_s$ );
7   else
8     stackit = true;
9 if stackit then
10  if  $n_s$  is leaf then
11    if  $p_i$  is leaf then
12      cache_neighbours( $p_i, n_s$ );
13    else
14      push ( $p_{i+1}, n_s$ ) onto stack;
15  else
16    if  $p_i$  is leaf then
17      push ( $p_i, n_s l$ ) onto stack;
18      push ( $p_i, n_s r$ ) onto stack;
19    else
20      push ( $p_{i+1}, n_s l$ ) onto stack;
21      push ( $p_{i+1}, n_s r$ ) onto stack;

```

4. Results

We present tests and benchmarks of our SFMM implementation to measure its precision and numerical performance. All tests here were performed using the Grenoble University supercomputer using Xeon Gold 6244 nodes (16 cores), except for the common-envelope evolution benchmark (Sect. 4.3), which was performed using 48 cores on a single AMD EPYC 9754 processor in the internal computing cluster of the Heidelberg Institute for Theoretical Studies.

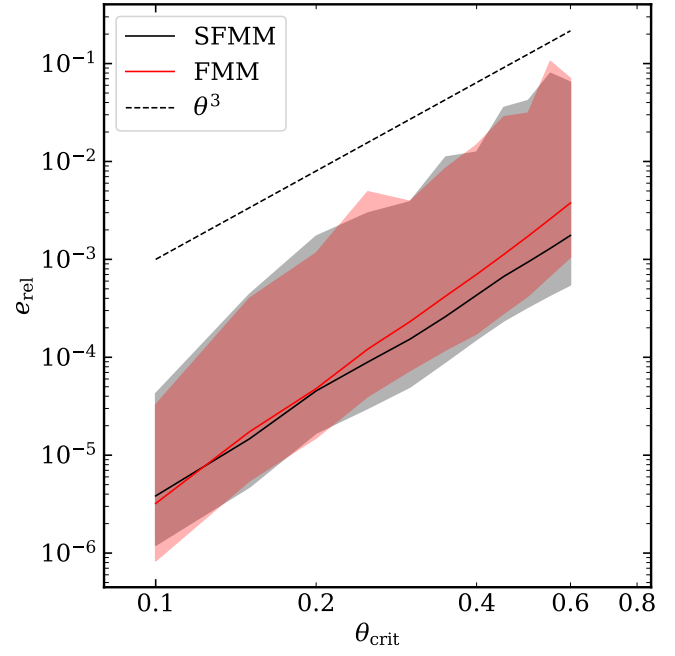
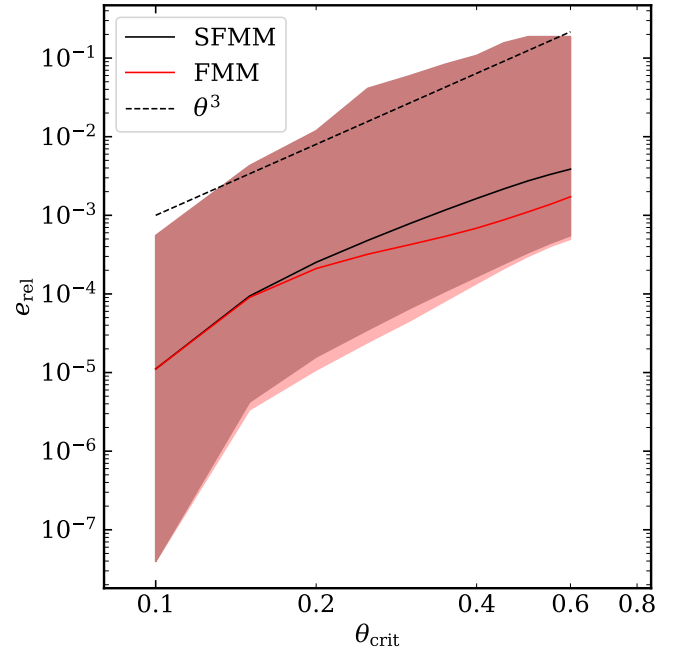


Fig. 2: Mean relative error (compared to a direct sum) versus the maximum opening angle computed in a Plummer sphere (top) and a homogeneous sphere (bottom) of 10^5 equal-mass particles, comparing FMM (red) to SFMM (black). The range boundaries around each curve represent the maximum error (upper) and the tenth percentile (lower). The close overlap between both methods suggests a similar overall accuracy.

4.1. Plummer and homogeneous sphere

First, we computed gravitational accelerations for particles placed in a Plummer sphere (Plummer 1911), comparing the previous and new algorithms. We generated a randomly drawn distribution of 10^5 equal-mass particles placed (as described in Price & Monaghan 2007) to achieve the density profile of a

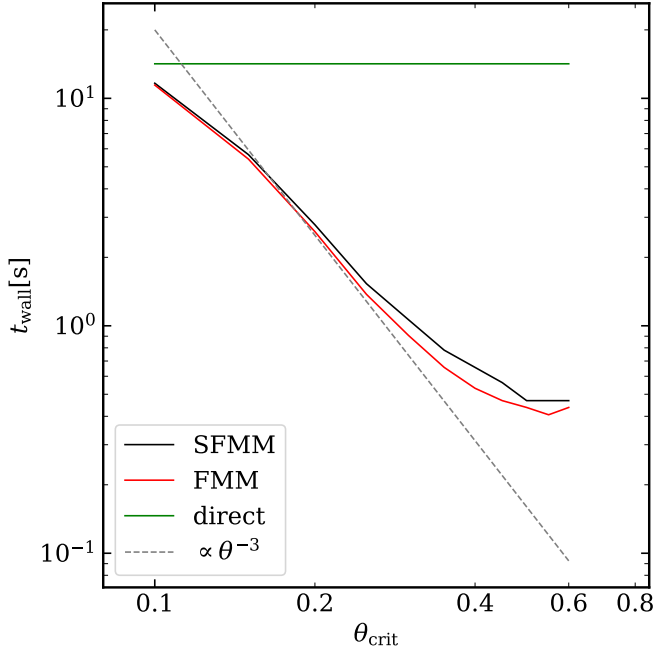


Fig. 3: Wall time (in seconds) spent computing gravitational forces in a Plummer sphere of 10^5 particles for a range of maximum opening angles. The two multipole methods are shown in red (FMM) and black (SFMM). The reference time of the direct algorithm is plotted in green and is unrelated to the critical opening angle.

Plummer sphere

$$\rho(r) = \frac{3Ma^2}{4\pi(a^2 + r^2)^{\frac{5}{2}}}, \quad (31)$$

where $M = 1$ (code units) is the total mass and $a = 1$ (code units) is the characteristic radius, also called Plummer radius. Gravitational forces were computed with both methods for eleven different maximum opening angle criteria $\theta_{\text{crit}} \in [0.1, 0.6]$ with 0.05 step increments. We compared these forces to those computed with a direct sum.

Figure 2 (top) shows the mean relative error ($e_{\text{rel}} \equiv 1/N \sum_i |a_i - a_{i,\text{directsum}}| / |a_{i,\text{directsum}}|$) over the whole θ_{crit} range, comparing the SFMM scheme (black line/dark red shading) to the FMM scheme (red line/light red shading). The shadings represent the spread of errors between the maximum and the tenth percentile. The two methods give similar results for small θ_{crit} . SFMM gives 1.2 to 2.4 times less accurate mean values compared to FMM from $\theta_{\text{crit}} = 0.2$ to the end of the range. However, both methods give an almost identical range of errors. Maximum errors are strictly identical, and tenth percentiles (lower bound of the shaded region) are within a factor of 0.4.

The lower panel of Figure 2 shows the corresponding results for a homogeneous density sphere. In this case, the SFMM gives a better mean error for the whole range of θ_{crit} , and the overall error range is one order of magnitude below the Plummer distribution. This implies that the difference between the two methods here mainly comes from how and how many nodes are opened, which depends on the particle distribution.

In terms of performance, Figure 3 represents the wall time in seconds for SFMM (black line) and FMM (red line) as a function of the critical opening criterion. The direct sum algorithm is

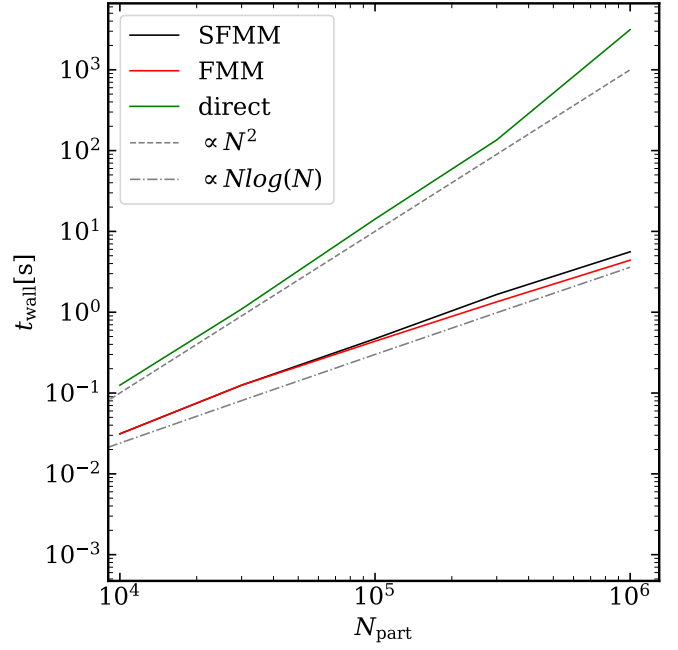


Fig. 4: Wall time (in seconds) spent computing gravitational forces in a Plummer sphere with 10^4 to 10^6 particles with $\theta_{\text{crit}} = 0.5$. The two multipole methods, FMM in red and SFMM in black, are compared to the direct sum algorithm in green. Both multipole method follows their expected $\mathcal{O}(N \log N)$ scaling while the direct sum is several order of magnitude more computationally expensive following a $\mathcal{O}(N^2)$.

also shown as a reference. Wall times roughly follow θ^{-3} (dashed line) up to $\theta = 0.4$ for both methods. This comes from the number of nodes opened during a tree walk, which is proportional to θ^{-3} . However, these slopes flatten as θ_{crit} increases up to 0.6. The difference is roughly constant over the explored θ_{crit} range, with the SFMM being 12% slower on average than the previous methods. The two methods are closer in computational cost with large values of opening angle, with the SFMM only 7% slower with $\theta_{\text{crit}} = 0.5$, which is the default value we adopt in PHANTOM.

Figure 4 shows the wall time for the direct sum (green line), FMM (red line) and SFMM (black line) for a range between 10^4 and 10^6 particles with $\theta_{\text{crit}} = 0.5$. Our new implementation of the SFMM (Algorithm 1) follows the same scaling law, $\mathcal{O}(N \log N)$ (dotted dashed line) as the original method with between 7% and 26% extra computational cost $N_{\text{part}} > 10^5$.

4.2. Binary polytrope test

We computed the evolution of a binary star modelled by two polytropes to emphasise the conservation properties of our new SFMM algorithm. We initialised a primary star of $1 M_{\odot}$ and $1 R_{\odot}$ and its companion of $0.314 M_{\odot}$ and $0.680 R_{\odot}$ (equal density), set up using the automated Relax-O-Matic™ procedure in PHANTOM (Appendix C of Lau et al. 2022a). The two gaseous spheres are set orbiting around each other in a circular orbit with a semi-major axis equal to 0.05 au. The mass resolution was set to $10^{-4} M_{\odot}$ giving a total particle number around 1.3×10^4 . We used an ideal gas equation of state with $\gamma = 5/3$ to model the polytropes. During this test, the binary motion was integrated during twenty of its orbits with the original FMM and our new SFMM.

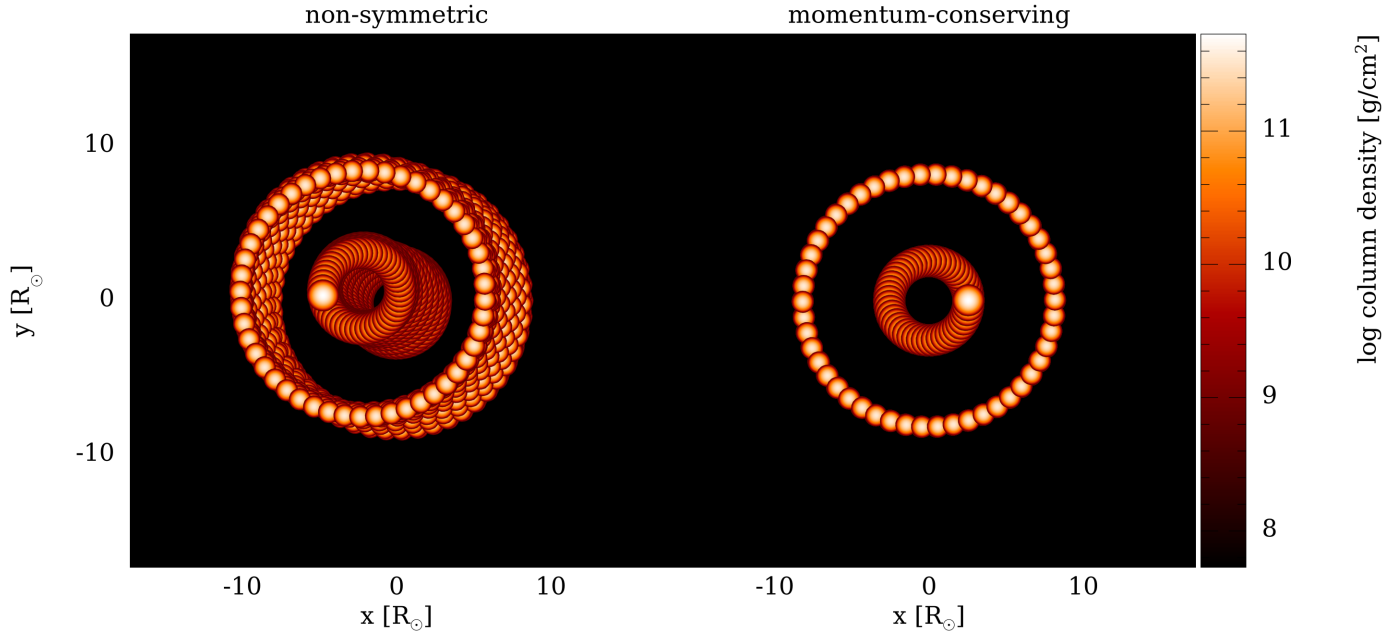


Fig. 5: Twenty orbits of a binary system of polytropic stars. The render of the logarithmic column density of each timestep is stacked to construct the path of the binary components. With the non-symmetric tree (left), a small but accumulative non-conservation error causes the orbit to drift with time, while this drift is removed with the new implementation (right).

Figure 5 shows logarithmic column density renderings of the binary, stacked and displayed for both methods at intervals of 1% of the orbital period. The plot shows the trajectory of both stars over the 20 orbits. The non-symmetric force evaluations computed with the FMM generate a visible drift of the binary barycentre (left panel) that is not present with the SFMM version (right panel). With FMM, the centre-of-mass can be seen to drift (to the upper left in the figure) by a significant fraction of the semi-major axis. By contrast, the binary trajectory stays stable during the whole simulation with our new SFMM. The SFMM calculation also shows a perfect orbital phase recovery, with the final position of the stars perfectly superimposed with their initial location. By comparison, the non-symmetric version does not conserve this property.

Figure 6 shows the corresponding evolution in time of both linear (top) and angular (bottom) momentum of the two simulations reported in code units ($G = M_\odot = au = 1$). The linear momentum deviation (relative to zero; top panel) never exceeds a value of 10^{-13} with SFMM, consistent with conservation to machine precision, while the previous method rises to 10^{-2} over the 20 orbital periods simulated. The SFMM still shows fluctuations in angular momentum around the initial value with a standard deviation of 2.0×10^{-5} (black line in bottom panel). However, no clear drift is visible throughout the entire evolution. By contrast, the previous version shows an angular momentum drift over the simulation, while the fluctuations show a larger standard deviation of 2.2×10^{-4} (red line in lower panel).

4.3. Common-envelope evolution

To demonstrate the capabilities of the SFMM algorithm on a more complex, self-gravitating astrophysical problem, we compare the original FMM and the new SFMM in a simula-

tion of common-envelope evolution. Common-envelope evolution is a phase in the evolution of a binary star where one star (the donor) engulfs its much more compact companion (the accretor) as it expands as a giant star (Paczynski 1976; Ivanova et al. 2013; Röpke & De Marco 2023; Schneider et al. 2025). The companion and the giant star’s core orbit each other inside the tenuous giant envelope, where drag forces cause them to spiral inwards over several orbits. Some or all of the giant envelope is ejected in this process. Common-envelope evolution has been simulated extensively with PHANTOM (Iaconi et al. 2017, 2019; Reichardt et al. 2019, 2020; Lau et al. 2022a,b; González-Bolívar et al. 2022, 2024; Bermúdez-Bustamante et al. 2024; Lau et al. 2025; Nibbs et al. 2025). We use the same setup and method as Lau et al. (2022a) for the “gas + radiation” equation of state that assumes radiation to be in thermodynamic equilibrium with the gas and for the “low-resolution” case that only uses 50,000 SPH particles.

Figure 7 shows a comparison between the simulations performed with the FMM and with the SFMM. The first row shows snapshots taken during the dynamical spiral-in phase of the stellar cores, which are visually indistinguishable between the two methods. The second row shows a phase in the late-time evolution after much of the original giant envelope has dispersed and some parts have been ejected. An exact match between the two methods is no longer possible as turbulent, convective flows have developed in the ejecta, which amplify small deviations exponentially.

Figure 8 compares the evolution in total linear and angular momentum between the FMM and SFMM. A similar improvement in linear momentum conservation is observed compared to the binary polytrope test. The simulation was set up to have zero linear momentum initially. With the FMM, total momentum is conserved to within 10^{-4} (in code units) and to within 10^{-13} with the SFMM, the latter consistent with conservation to round-off

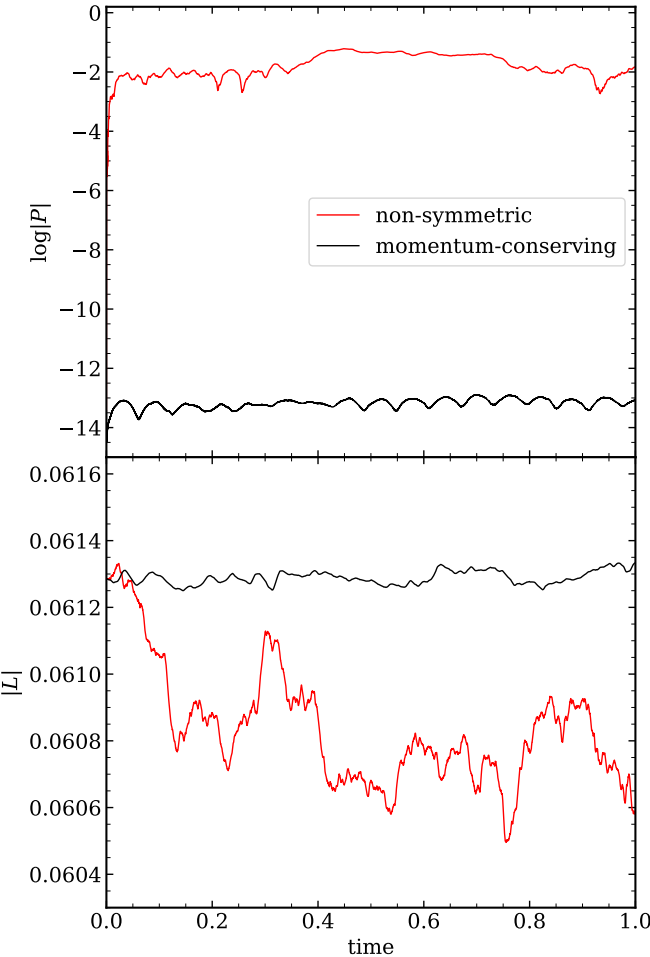


Fig. 6: Evolution of the linear momentum (top) and angular momentum (bottom) of a binary system of polytropic stars over 20 orbits. The non-symmetric FMM and SFMM are plotted respectively in red and black. The linear momentum in the SFMM case is conserved up to machine precision over the whole simulation. Angular momentum conservation is also improved with the SFMM.

error. There is no discernable difference in computational cost. With the new method, the centre-of-mass drift is restricted to within $\sim 10^{-10} R_\odot$ in the first ten years, whereas it used to be $\sim 10^{-1} R_\odot$. Figure 8 also shows that the FMM and SFMM conserve angular momentum to a similar level of 10^{-4} over thirty years.

Conserving total angular and linear momentum is especially important for capturing the orbital dynamics after the initial fast plunge-in. In this phase, the secular orbital evolution is influenced by gravitational interaction with the remaining bound envelope, and the morphology and velocity of bipolar outflows and jets could be highly sensitive to small drifts in the barycentre.

Figure 9 compares the key results in a simulation of common-envelope evolution: the evolution in the amount of unbound envelope mass and the separation between the giant core and the companion. Due to excellent angular momentum conservation in both the FMM and SFMM, there are only minor differences in the evolution of orbital separation and almost no discernable difference up to the immediate end of the plunge-in phase ($t \approx 4$ yr). There are larger differences ($\sim 10\%$) observed in the amount of bound envelope mass after the plunge-in. As

noted earlier, because turbulent flows develop in this phase, an exact match between the two simulations is not expected. In this case, the difference in the amount of bound mass is mainly due to a time offset at $t = 5 - 6$ yr of the onset of a faster phase of mass ejection. The simulations record nearly identical values of bound mass beyond $t = 15$ yr.

5. Discussion

The tests presented in this study highlight the advantages of symmetrising our previous self-gravity scheme. Conserving linear momentum up to machine precision allows a better physical description of the studied system as shown with the binary polytrope test (see Figure 5). This eliminates the centre of mass drift discussed in Potashov & Yudin (2024) visible with the previous method for any θ_{crit} . Improved momentum conservation also improves the accuracy of other quantities, such as the orbital phase and the angular momentum. In principle, it is also possible to adapt the SFMM method to also conserve angular momentum to machine precision, although this involves computing and storing octupole moments (Marcello 2017). It is unclear to us whether the gain would be worth the additional computational cost.

In general, the precision of multipole methods is constrained by the expansion order and the maximum opening angle. However, the node-opening criterion will also affect the measured accuracy. We found that the SFMM approximation seems to be slightly more sensitive to peaked distributions like the Plummer sphere.

We explain this higher sensitivity by two main factors: First, a Plummer distribution gives a strongly unbalanced tree due to its large spatial extension and the sharp density drop at its outskirts. The leaf size distribution (i.e. depth of the tree) then reflects the inverse of the density profile, giving a large number of small leaf nodes in the tree core and very few large leaf nodes at the outskirts. Consequently, the SFMM algorithm will find many interactions with strongly different node sizes. As shown in Springel et al. (2021), the SFMM approximation gives the worst error with large size differences between interacting nodes. This effect increases as the maximum opening angle rises, allowing interactions in shallower parts of the tree. Our patch described in Section 3 to force nodes of the level to only interact with themselves is inefficient in avoiding such unbalanced interactions if the sizes are too spread across levels in the tree.

Additionally, as the MAC numerator is spread across the target and source node, SFMM intrinsically allows more interactions to be well-separated in a fixed-size system (the maximum denominator is bound by the system size). This amplifies the accumulation of unbalanced interactions, resulting in a larger overall mean error. A homogeneous sphere distribution has similar leaf node sizes across the whole system. The mean error is lower for both methods. However, the non-symmetric interactions in FMM will inevitably give a less precise result than SFMM in this case. Despite this sensitivity, the SFMM does not show larger maximum errors compared to FMM.

The structure of our new algorithm closely follows the previous implementation in PHANTOM as described in Price et al. (2018). The symmetrisation thus required only small changes in the codebase. The underlying aim was to ensure similar performance and scaling by keeping the self-gravity calculation done alongside the SPH force routine, rather than done separately as in the GADGET implementation (Springel et al. 2021).

The parallelisation strategy also remained the same, which again saved development effort. This conservative choice required introducing work duplication in the self-gravity solver

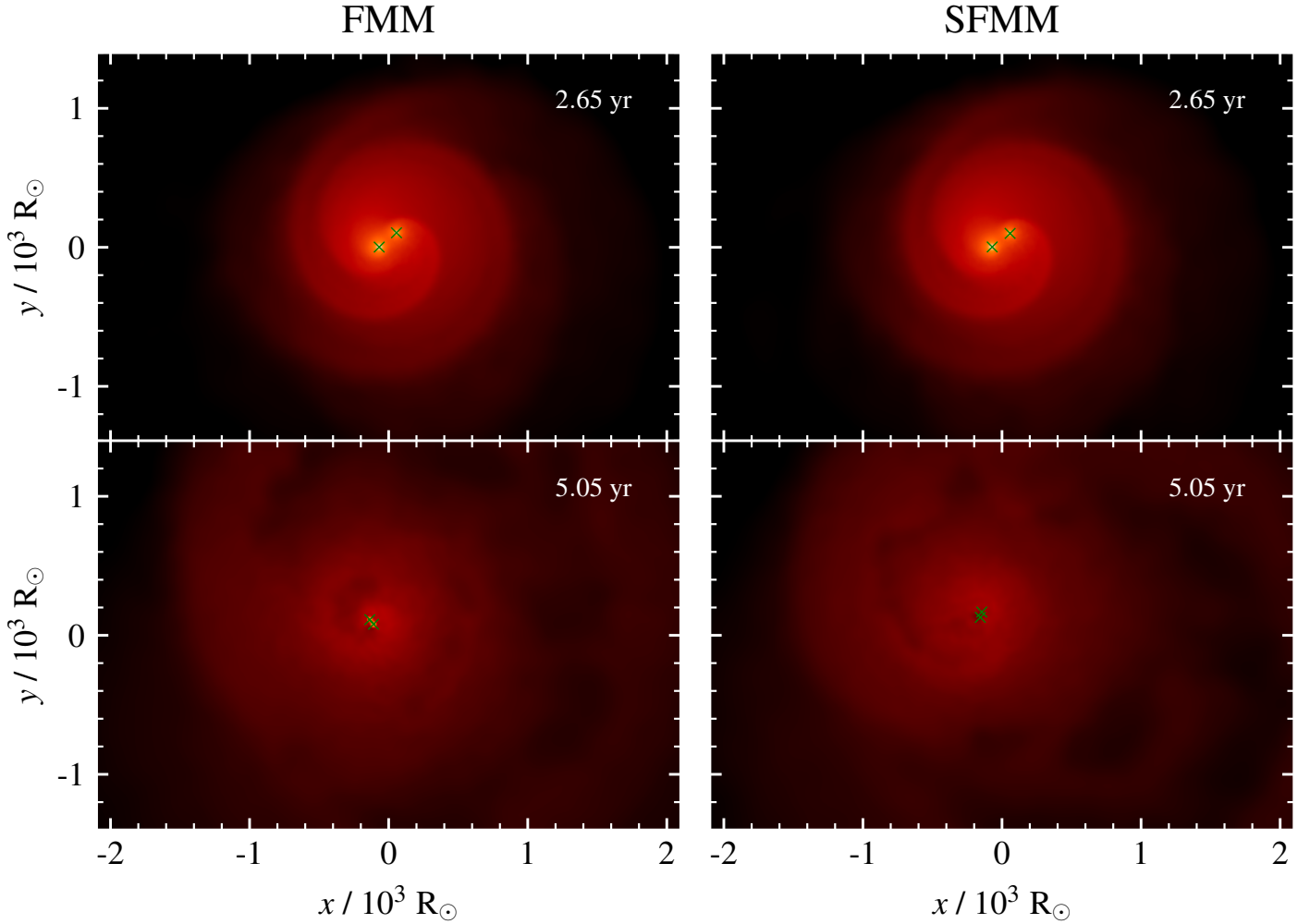


Fig. 7: Density slices at $t = 2.65, 5.05$ yr in the orbital plane of a simulation of common-envelope evolution, comparing results obtained with the momentum-conserving method (right) with those obtained with the previous non-symmetric method (left). The green crosses show the positions of the point masses representing the stellar core and the companion star. The results are indistinguishable up to the end of the plunge-in where the ejecta becomes turbulent. Plot was made using the SARRACEN Python library (Harris & Tricco 2023).

with the cost of losing the $O(N)$ scaling of the SFMM. This may seem counterproductive. However, our tests show comparable performance similar to the previous self-gravity solver. It demonstrates that this duplication strategy can efficiently absorb the extra calculations while not impacting the parallel scaling.

That being said, further optimisation of the algorithm may be possible to reach or outperform the previous implementation. The long-range interaction evaluation in the new algorithm costs around 50% of the CPU time. However, the shared long-range interactions could be cached amongst threads. That way, theoretically, only one thread would actually compute a specific interaction, and all other threads requiring it would fetch it from a cache. This optimisation takes advantage of the shared interactions only available in the SFMM. This can alleviate parts of the work duplication, resulting in better scaling. Another optimisation could use the symmetric interactions to only compute one side of them (Dehnen 2002). However, such optimisations require more complex synchronisations in the parallel loops with read and write operations on shared caches that may trade-off against parallel performance, and should therefore be approached with caution.

6. Conclusions

We implemented a new parallel algorithm based on Dehnen (2000) that symmetrises the fast multipole method with adaptive gravitational softening in PHANTOM. By construction, this symmetrisation ensures that linear momentum is conserved to machine precision while still using multipole expansions to approximate the self-gravity. Our tests demonstrate that this is achieved in practice. Specifically, we find:

- (i) The new method gives similar accuracy of gravitational accelerations compared to the previous default method in PHANTOM, although this depends on the exact distribution of particles.
- (ii) Our new method eliminates centre of mass drift in stellar orbits and common envelope simulations while giving similar observables like the orbital separation or the bound mass to the previous tree-based gravity solver implemented in PHANTOM.
- (iii) We modified the dual tree traversal to check and compute node-node interactions in parallel on individual branches connecting leaf nodes to the tree root. We also introduce a modified acceptance criterion to correctly account

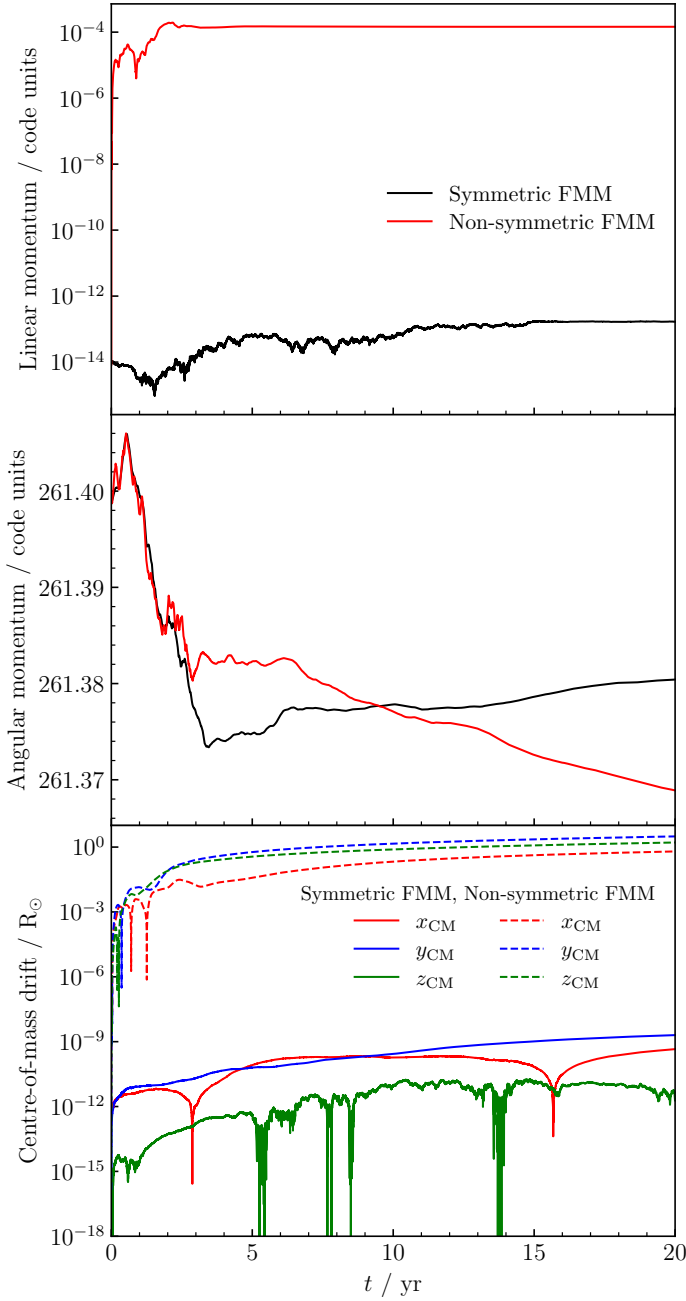


Fig. 8: Similar to Figure 6, but for the problem of simulating common-envelope evolution. Bottom panel compares the x , y , and z -centre-of-mass drifts between the SFMM and FMM.

for adaptive gravitational softening without changing the Green's function in multipole expansions. This allowed us to implement the new traversal in the existing codebase without changing the parallelisation strategy.

- (iv) We avoid the need for task-based parallelism by introducing work duplication. This trades the notional $\mathcal{O}(N)$ scaling for $\mathcal{O}(N \log N)$ but with efficient sharing of the workload across the whole tree, resulting in comparable parallel performance to the previous method without thread locking.

While further optimisations of the method may be possible, the overall accuracy and numerical performance of our new implementation, in addition to its perfect momentum conservation, already offer advantages over the existing method. The new method is therefore now the default solver available in PHANTOM.

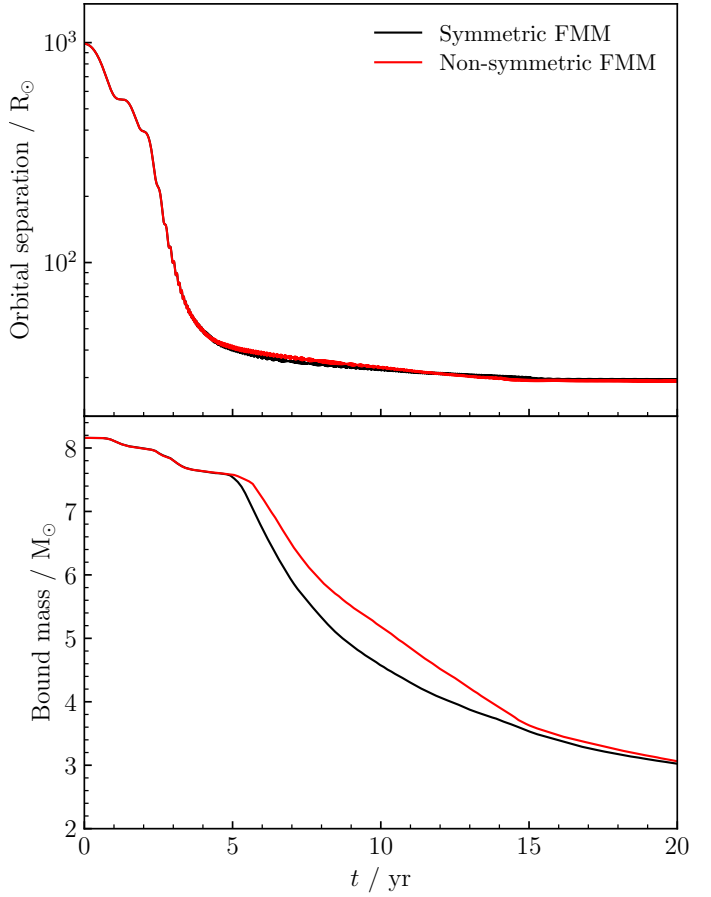


Fig. 9: Comparison of key results between the SFMM and FMM for the common-envelope evolution simulation. Top panel: Separation between the companion and the donor star's core. Bottom panel: Total envelope mass that is bound, that is, possessing a negative sum of kinetic and potential energies.

Acknowledgements. We thank Walter Dehnen, Matthew Bate and Estelle Moraux for useful discussions. All the computations presented in this paper were performed using the GRICAD infrastructure (<https://gricad.univ-grenoble-alpes.fr>), which is supported by Grenoble research communities. M. Y. M. L. acknowledges funding by the European Union (ERC, ExCEED, project number 101096243). Views and opinions expressed are, however, those of the authors only and do not necessarily reflect those of the European Union or the European Research Council Executive Agency. Neither the European Union nor the granting authority can be held responsible for them. DP also thanks IPAG, CNRS, Université-Grenoble-Alpes, François Ménard, Nicolas Cuello and the ODYSSEY/Stellar-MADE teams for hosting and support during his sabbatical in Grenoble, where this work was completed. His visit was made possible by funding from the Campagne d'accueil de scientifiques étrangers – UGA et Grenoble INP-UGA – Année 2025 and by European Union funding of the Stellar-MADE (project number 101042275) and DUST2PLANETS (project number 101053020) ERC projects.

References

- Barnes, J. & Hut, P. 1986, Nature, 324, 446
- Bate, M. R. & Burkert, A. 1997, MNRAS, 288, 1060
- Benz, W., Bowers, R. L., Cameron, A. G. W., & Press, W. H. . 1990, ApJ, 348, 647
- Bermúdez-Bustamante, L. C., De Marco, O., Siess, L., et al. 2024, MNRAS, 533, 464
- Capuzzo-Dolcetta, R. & Miocchi, P. 1998, J. Comp. Phys., 143, 29
- Dehnen, W. 2000, ApJ, 536, L39
- Dehnen, W. 2002, J. Comp. Phys., 179, 27
- Dehnen, W. 2014, Computational Astrophysics and Cosmology, 1, 1
- Dubinski, J. 1996, New A, 1, 133

Gafton, E. & Rosswog, S. 2011, MNRAS, 418, 770

Gingold, R. A. & Monaghan, J. J. 1977, MNRAS, 181, 375

González-Bolívar, M., De Marco, O., Bermúdez-Bustamante, L. C., Siess, L., & Price, D. J. 2024, MNRAS, 527, 9145

González-Bolívar, M., De Marco, O., Lau, t., Hirai, R., & Price, D. J. 2022, MNRAS, 517, 3181

Greengard, L. & Rokhlin, V. 1987, J. Comp. Phys., 73, 325

Harris, A. & Tricco, T. 2023, The Journal of Open Source Software, 8, 5263

Hernquist, L. & Katz, N. 1989, ApJS, 70, 419

Hubber, D. A., Batty, C. P., McLeod, A., & Whitworth, A. P. 2011, A&A, 529, A27

Iaconi, R., Maeda, K., De Marco, O., Nozawa, T., & Reichardt, T. 2019, MNRAS, 489, 3334

Iaconi, R., Reichardt, T., Staff, J., et al. 2017, MNRAS, 464, 4028

Ivanova, N., Justham, S., Chen, X., et al. 2013, A&A Rev., 21, 59

Iwasawa, M., Oshino, S., Fujii, M. S., & Hori, Y. 2017, PASJ, 69, 81

Lau, M. Y. M., Hirai, R., González-Bolívar, M., et al. 2022a, MNRAS, 512, 5462

Lau, M. Y. M., Hirai, R., Price, D. J., & Mandel, I. 2022b, MNRAS, 516, 4669

Lau, M. Y. M., Hirai, R., Price, D. J., Mandel, I., & Bate, M. R. 2025, A&A, 699, A274

Lucy, L. B. 1977, AJ, 82, 1013

Marcello, D. C. 2017, AJ, 154, 92

Monaghan, J. J. & Lattanzio, J. C. 1985, A&A, 149, 135

Nibbs, J., De Marco, O., Siess, L., Hirai, R., & Price, D. 2025, arXiv e-prints, arXiv:2512.16225

Paczyński, B. 1976, in IAU Symposium, Vol. 73, Structure and Evolution of Close Binary Systems, ed. P. Eggleton, S. Mitton, & J. Whelan, 75

Plummer, H. C. 1911, MNRAS, 71, 460

Potashov, M. S. & Yudin, A. V. 2024, Numerical Methods and Programming, 25, 396

Price, D. J. & Monaghan, J. J. 2007, MNRAS, 374, 1347

Price, D. J., Wurster, J., Tricco, T. S., et al. 2018, PASA, 35, e031

Reichardt, T. A., De Marco, O., Iaconi, R., Chamandy, L., & Price, D. J. 2020, MNRAS, 494, 5333

Reichardt, T. A., De Marco, O., Iaconi, R., Tout, C. A., & Price, D. J. 2019, MNRAS, 484, 631

Röpke, F. K. & De Marco, O. 2023, Living Reviews in Computational Astrophysics, 9, 2

Salmon, J. K. & Warren, M. S. 1994, J. Comp. Phys., 111, 136

Schaller, M., Borrow, J., Draper, P. W., et al. 2024, MNRAS, 530, 2378

Schneider, F. R. N., Lau, M. Y. M., & Roepke, F. K. 2025, arXiv e-prints, arXiv:2502.00111

Springel, V. 2005, MNRAS, 364, 1105

Springel, V., Pakmor, R., Zier, O., & Reinecke, M. 2021, MNRAS, 506, 2871

Springel, V., Yoshida, N., & White, S. D. M. 2001, New A, 6, 79

Steinmetz, M. & Mueller, E. 1993, A&A, 268, 391

Wadsley, J. W., Keller, B. W., & Quinn, T. R. 2017, MNRAS, 471, 2357

Wadsley, J. W., Stadel, J., & Quinn, T. 2004, New A, 9, 137

Wetzstein, M., Nelson, A. F., Naab, T., & Burkert, A. 2009, ApJS, 184, 298

Appendix A: Moment translation formulae

A.1. Mass Moment translation

The methods presented above need to compute the mass moments of nodes defined in the system domain to proceed to the multipole expansion of the Green's function. While it is possible to compute any mass moment of a node by only providing its particle set and centre. Nodes in hydrodynamical simulations are typically organised in a hierarchical tree to optimise neighbour search. Hence, nodes corresponding to internal nodes of the tree share their set of particles with their children. In such a configuration, it is numerically more efficient to compute only the mass moment on the children and translate them to the parent centre, summing the contribution of each of them. Using this translation method, the moment of the parent node B' is

$$Q_n^{B'} = \int_V \rho(\mathbf{x}_j) \mathbf{b}'^{(n)} d^3x \quad (\text{A.1})$$

$$= \int_V \rho(\mathbf{x}_j) (\mathbf{g} + \mathbf{b})^{(n)} d^3x \quad (\text{A.2})$$

$$= \int_V \rho(\mathbf{x}_j) \underbrace{(\mathbf{g} + \mathbf{b}) \otimes \cdots \otimes (\mathbf{g} + \mathbf{b})}_{n \text{ times}} d^3x_j. \quad (\text{A.3})$$

where \mathbf{g} is the vector between child and parent centre and \mathbf{b} is the distance between a mass element and the centre of the child. The mass moment can then be computed only on the leaf nodes and then translated into every internal node of the tree in a bottom-up fashion.

A.2. Gravitational moment translation

When the multipole expansion is used to compute gravitational moments between pairs of nodes, the gravitational forces are passed down to every particle in a node. The simplest solution would be to proceed like that for every node in the domain. However, as mentioned above, when the symmetric fast multipole method is used, internal node-node interactions contribute to the long-range interactions of leaf nodes. In such a case, it is numerically more efficient to translate gravitational moments and propagate them downward through the tree, node to node, down to the leaf nodes and then to the particles.

To find the gravitational moment translation formula, we can express the FMM force as a function of the 3 vectors involved in the expansion

$$f_g(\mathbf{a}_i, \mathbf{r}, \mathbf{b}_i) = \sum_{k=0}^p \frac{\mathbf{a}_i^{(k)}}{k!} \cdot (-1)^k \underbrace{\sum_{n=0}^{p-k} \frac{1}{n!} D_{n+k+1}(\mathbf{r}) \cdot Q_n^B(\mathbf{b}_i)}_{dM_k(\mathbf{r}, \mathbf{b}_i)}. \quad (\text{A.4})$$

Using a shifted centre of the box $\mathbf{a} = \mathbf{h} + \mathbf{a}'$, we want that

$$f_g(\mathbf{a}'_i, \mathbf{r}', \mathbf{b}_i) = f_g(\mathbf{a}_i, \mathbf{r}, \mathbf{b}_i) \quad (\text{A.5})$$

$$= \sum_{k=0}^p \frac{(\mathbf{a}'_i + \mathbf{h})^{(k)}}{k!} \cdot dM_k(\mathbf{r}, \mathbf{b}_i) \quad (\text{A.6})$$

$$= \sum_{k=0}^p \frac{\mathbf{a}'_i^{(k)}}{k!} \underbrace{\sum_{l=k}^p \frac{1}{(l-k)!} \mathbf{h}^{(l-k)} \cdot dM_l(\mathbf{r}, \mathbf{b}_i)}_{dM_k(\mathbf{r}', \mathbf{b}_i)}. \quad (\text{A.7})$$

We define then the translated gravitational moment as being

$$dM_k(\mathbf{r}', \mathbf{b}_i) = \sum_{l=k}^p \frac{1}{(l-k)!} \mathbf{h}^{(l-k)} \cdot dM_l(\mathbf{r}, \mathbf{b}_i), \quad (\text{A.8})$$

under a translation of the centre by a vector \mathbf{h} . However, it is worth noting this formula is not exact since it would require a Taylor expansion of D_{n+k+1} , which would require the order $2p$ of the Green's functions moments. In reality, this translation operation gives the same result as the direct method up to the floating-point error.